Computer Physics Communications 135 (2001) 176–189

Computer Physics Communications

www.elsevier.nl/locate/cpc

The earth regeneration effect of solar neutrinos: a numerical treatment with three active neutrino flavors ☆

Jai Sam Kim *, Kyungsoo Lee

Department of Physics, Pohang University of Science and Technology, Pohang 790-784, South Korea

Received 28 August 2000

Abstract

We introduce an integrated algorithm for full scale investigation of the earth regeneration effect of solar neutrinos with all three active neutrinos. We illustrate that the earth effect on low energy solar neutrinos ($E_\nu < 20$ MeV) causes large variations in the survival probabilities for large values of the mixing angle θ_{12} at given θ_{13}. But it is maximal for small values of θ_{13} and diminishes for large values at given θ_{12}. The nadir angle dependence is sensitive to the value of $E' \equiv E/\Delta_{12}$. We also show that for large values of θ_{13}, the earth effect is significant for high energy neutrinos ($E' > 10^9$). We use a few sample iso-SNU contour plots to show that combination of the seasonal variations of Ga data and the D/N difference of water data can lead to determination of the three mixing parameters, Δ_{12}, θ_{12}, θ_{13} decisively.

PACS: 14.60.Pq; 26.65.+t; 96.60.Jw

1. Introduction

Neutrinos are produced abundantly from thermonuclear reactions taking place in the stellar core. They carry away most of the energy during the supernova explosion. Due to the extreme weakness of its interaction it escapes its cradle almost intact and provides us with most reliable clues to the internal physical environments of a star. Thus neutrino astronomy has been established as an important research field recently. The Standard Solar model (SSM) [1–3] predicts the flux of the electron neutrino. The historic Homestake experiment [4] for detecting solar neutrinos revealed that the detected neutrinos fall far short of the SSM prediction.

Several mechanisms were proposed for the depletion of solar neutrinos. Pontecorvo [5] proposed the idea of neutrino flavor oscillation earlier than any unification theories [6]. (See Ref. [7] for an interesting review.) The possibility of solar neutrino flux reduction by vacuum oscillation was investigated earlier [8, 9]. Subsequent experiments [10–13] revealed that the solar neutrino deficit depends on the energy of the neutrino. Recently the idea of flavor oscillation combined with the Mikheyev–Smirnov–Wolfenstein (MSW) effect [14,15] has been most popular. The MSW equations have been vigorously studied. For simple matter densities, some authors [16–20] derived accurate analytic solutions for the two-neutrino MSW evolution equations. These solutions have been used for computing the neutrino survival probabilities with the approximation of the solar matter density by a mosaic of exponential functions. Direct numerical analysis was

☆ This work was funded by POSTECH research fund.

* Corresponding author.
E-mail address: jsk@postech.ac.kr (J.S. Kim).

0010-4655/01/$ – see front matter
PII: S0010-4655(00)00237-X

carried out also [21]. Two-flavor MSW solutions to the solar neutrino puzzle were fully analyzed with high accuracy, including both the day/night effect and spectral information [22,23].

Recent Super-Kamiokande experiment [24] shows an evidence for oscillations of the atmospheric neutrinos [25–28]. The data are in good agreement with two-flavor $\nu_\mu \leftrightarrow \nu_\tau$ oscillations. These results did establish that neutrinos oscillate and possess nonzero masses. Thus full three-flavor neutrino oscillation analysis is needed for more accurate estimation of neutrino masses and mixing angles. Even four neutrino solutions with the sterile neutrino have been suggested [29–34].

It has been argued [35–37] that under certain conditions the solution of the solar neutrino evolution equation in the two neutrino case can be extended to the three neutrino case with a slight modification. There have been many analytic works on three-flavor MSW solutions of the solar neutrino problem with simple linear and exponential matter densities [35–42]. Most three-flavor MSW fits to the solar neutrino experiments have been made within the above framework [43–48]. Recently exact solutions to the three neutrino MSW equations for such simple matter densities were derived [49–51]. Direct numerical analysis is always desirable but it has been hampered by the huge computational costs. Recently we presented an efficient numerical algorithm for direct computation of the solar neutrino survival probability with all three active neutrinos [52,53].

According to the PREM model [54], the earth consists of 10 layers of different matter densities and compositions. The PREM model gives the matter density in each earth layer as a polynomial in radius. It is around $\rho = 1.6\sim6.1$ mol/cm^3. In such matter densities, the MSW effect can be significant for neutrinos with certain energies. The earth regeneration effect for solar neutrinos was numerically analyzed by many people within the two-flavor framework [55–66]. Since numerical analysis takes a lot of computing time a few attempts to derive analytic formula were made. Approximating the matter density in each of the five simplified earth layers as an even degree quartic polynomial in radius, Lisi and Montanino [67] derived analytic solutions for the two-neutrino MSW equations. Other attempts were made for three neutrino MSW equations with a periodic step-function density profile [68] and with constant matter densities [69]. There have been direct numerical works [70] on the earth regeneration effect with all three neutrinos but it was not carried enough to the depth as done in the two flavor case.

In this paper we present an integrated algorithm for analyzing the earth regeneration effect of solar neutrinos with all three active neutrinos considered. Integration of neutrino evolution equations can be done with any ordinary differential equation solver such as adaptive Runge–Kutta or Bulirsch–Stoer methods (see, e.g., [71]). The wavefunction of a neutrino passing through the earth oscillates rapidly with large amplitudes in certain ranges of energy and mixing parameters. The crux of the problem is how to take time averages out of these wildly oscillating wavefunctions. Two methods have been used in the two neutrino case. Baltz and Weneser [57] carefully analyzed the oscillatory behavior of the survival probabilities and derived a formula that uses instantaneous values of the two particular wavefunctions. Exploiting the symmetry of the transition probabilities, Smirnov [62] derived a formula that uses only one transition probability, $P(\nu_2 \to \nu_e)$. Due to economy of the Smirnov's formula it has been widely used. However, we could not extend the formula to the three neutrino case. There is no shortcut in this case and we need to integrate the evolution equation for three different initial conditions, we realized. We introduce a method to obtain time averages of survival probabilities of solar neutrinos after passing through the earth in the three neutrino case. Our method is numerical and thus quite general and can be used with any number of flavors.

This paper is organized as follows: In Section 2 we review the basic formalism very briefly. In Section 3 we introduce our method for taking averages of neutrino fluxes as they pass through the earth core. In Section 4 we illustrate the complexity of the earth effect occurring at large mixing angles. We illustrate how it depends on neutrino energies, the mixing parameters, and the nadir angles. In Section 5 we present how to make long term averages such as daily averages in different seasons and monthly and yearly averages. In Section 6 we present sample contour plots for an interesting set of parameters. We discuss characteristics of the sample contour plots. In Section 7 we summarize our works and suggest the

possibility that combination of the seasonal variations of Ga data and the D/N difference of water data can lead to determination of the three mixing parameters, Δ_{12}, θ_{12}, θ_{13} decisively.

2. Basic formalism

The state of a neutrino can be expressed either in the weak eigenstate basis $|\nu_\alpha\rangle$ or in the mass eigenstate basis $|\nu_i\rangle$. The unitary matrix U transforms the mass eigenstates into the weak eigenstates,

$$\nu_\alpha = \sum_{i=1}^{3} U_{\alpha i}\nu_i, \quad \alpha = e, \mu, \tau. \tag{1}$$

The Particle Data Group [72] adopts the convention for the mixing matrix,

$$U = \begin{pmatrix} C_1C_3 & S_1C_3 & S_3 \\ -S_1C_2 - C_1S_3S_2 & C_1C_2 - S_1S_3S_2 & C_3S_2 \\ S_1S_2 - C_1S_3C_2 & -C_1S_2 - S_1S_3C_2 & C_3C_2 \end{pmatrix}, \tag{2}$$

where $C_i \equiv \cos\theta_i$ and $S_i \equiv \sin\theta_i$ and the three mixing angles $\theta_1 = \theta_{12}$, $\theta_2 = \theta_{23}$, and $\theta_3 = \theta_{13}$ roughly measure mixing between mass eigenstates (1-2), (2-3), and (1-3), respectively. We have neglected the CP violating phase, which is irrelevant in this problem.

It is convenient to express the state of a neutrino as a mixture of three active neutrinos in the weak eigenstate basis,

$$\Phi(t) = a_e|\nu_e\rangle + a_\mu(t)|\nu_\mu\rangle + a_\tau(t)|\nu_\tau\rangle. \tag{3}$$

The mass matrix is non-diagonal in the weak eigenstate basis. It is obtained from the diagonal mass matrix,

$$M_{ij} = \sum_k U_{ik}^\dagger m_k^2 U_{kj}. \tag{4}$$

The wavefunctions $a_\alpha(t)$ of a neutrino in a medium obey the evolution equations,

$$\mathrm{i}\frac{\mathrm{d}}{\mathrm{d}t}\begin{pmatrix} a_e(t) \\ a_\mu(t) \\ a_\tau(t) \end{pmatrix} = \frac{1}{2\beta}\begin{pmatrix} M_{11} + A_c(t) & M_{12} & M_{13} \\ M_{21} & M_{22} & M_{23} \\ M_{31} & M_{32} & M_{33} \end{pmatrix}\begin{pmatrix} a_e(t) \\ a_\mu(t) \\ a_\tau(t) \end{pmatrix}, \tag{5}$$

where $A_c = 2\sqrt{2}G_F E N_e$ is added due to the interaction with the charged currents via the MSW mechanism [14,15] and $\beta = E/R_E$ (MeV/cm) and $t = R/R_E$.

In principle we can use the neutrino evolution equations in either of the two basis. In practice the mass eigenstate based equations require diagonalization of the mass matrix at each time step. Diagonalization introduces non-trivial errors and takes extra computing time in addition to the time to solve the ordinary differential equations. Thus we chose the weak eigenstate based evolution equations.

Let us make a quick check of the two neutrino resonant condition in the earth core where $N_e \simeq 0.466\rho$,

$$\cos(2\theta_{ij}) = \sqrt{2}\,G_F N_e/(\Delta_{ij}/2E), \tag{6}$$

while holding the other mixing angles equal to zero. One finds that for a small value of the (1-2) mixing angle ($\cos 2\theta_{12} \approx 1$), the (1-2) transition takes place for neutrinos with $E/\Delta_{12} \simeq 10^6 \sim 10^7$ eV^{-1}. For large values of θ_{12}, the resonant condition is satisfied for lower energy values. Thus the low energy *pp*-neutrinos can be susceptible to the earth matter.

3. Computational methods

The electron neutrinos born from various sources within the solar core come out to the solar surface with average probabilities [$X_e^2 \equiv P(\nu_e \to \nu_e)$, $X_\mu^2 \equiv P(\nu_e \to \nu_\mu)$, $X_\tau^2 \equiv P(\nu_e \to \nu_\tau)$]. In the interesting ranges of mixing parameters, Δ_{12}, θ_{12}, θ_{13}, we have compiled a large set of solar neutrino survival probabilities born at selected radial positions r with selected energies E [52,53]. We used $\Delta_{23} = 2.2 \times 10^{-3}$ eV^2 and $\theta_{23} = 43.5°$.

Integration of the neutrino evolution equations in the earth are carried out using the CERN library [73] routine DDEQBS, which is an implementation of the Bulirsch–Stoer algorithm. We used the PREM model [54] with $N_e = 0.466\rho$ in the core ($R <$

5463 km) and $N_e = 0.494\rho$ in the mantle. Our results agree with previous works [56,57,69]. We especially checked our results against those of [69] and found good agreements (see Fig. 1(a)). It would be extremely time-consuming to trace all these neutrinos individually as they pass through the earth. Instead we trace how three pure neutrinos, $\Psi_e(t = 0) = (1,0,0,0,0,0)$, $\Psi_\mu(t = 0) = (0,0,1,0,0,0)$ and $\Psi_\tau(t = 0) = (0,0,0,0,1,0)$ evolve as they pass through the earth for a given set of parameters, Δ_{12}, Δ_{23}, θ_{12}, θ_{13}, θ_{23}. We compile the wavefunctions for selected values of the energy E and the zenith angle η. Then we set up a handy interpolation function to be used for computing the neutrino fluxes arriving at various experiments in any given period of time.

Let us denote the states of pure neutrinos after passing through the earth as,

$$\begin{aligned}\Psi_e(t) &= \alpha_e(t)|\nu_e\rangle + \alpha_\mu(t)|\nu_\mu\rangle + \alpha_\tau(t)|\nu_\tau\rangle,\\ \Psi_\mu(t) &= \beta_e(t)|\nu_e\rangle + \beta_\mu(t)|\nu_\mu\rangle + \beta_\tau(t)|\nu_\tau\rangle,\\ \Psi_\tau(t) &= \gamma_e(t)|\nu_e\rangle + \gamma_\mu(t)|\nu_\mu\rangle + \gamma_\tau(t)|\nu_\tau\rangle.\end{aligned} \tag{7}$$

Then the state of a solar neutrino in a mixed state with probabilities, $(X_e^2, X_\mu^2, X_\tau^2)$ can be written as a linear sum of three pure states,

$$\begin{aligned}\Psi_{SE}(t) &= X_e \exp(\mathrm{i}\phi_1)\Psi_e(t) + X_\mu \exp(\mathrm{i}\phi_2)\Psi_\mu(t)\\ &\quad + X_\tau \Psi_\tau(t),\end{aligned} \tag{8}$$

where we assumed some phases for solar neutrinos while keeping the phase of the τ neutrino zero.

Let us denote the state of a solar neutrino arriving at the earth as,

$$\Psi_S(t=0) \equiv a_e|\nu_e\rangle + a_\mu|\nu_\mu\rangle + a_\tau|\nu_\tau\rangle. \tag{9}$$

Then the probability of a solar neutrino to emerge as an electron neutrino after passing though the earth is written as

$$\begin{aligned}P_{SE} &= \left|\langle\nu_e|\Psi_{SE}\rangle\right|^2 = |a_e\alpha_e + a_\mu\beta_e + a_\tau\gamma_e|^2\\ &= |a_e|^2|\alpha_e|^2 + |a_\mu|^2|\beta_e|^2 + |a_\tau|^2|\gamma_e|^2\\ &\quad + \left[a_e\alpha_e a_\mu^*\beta_e^* + \text{c.c.}\right] + \left[a_\mu\beta_e a_\tau^*\gamma_e^* + \text{c.c.}\right]\\ &\quad + \left[a_\tau\gamma_e a_e^*\alpha_e^* + \text{c.c.}\right].\end{aligned} \tag{10}$$

In order to obtain the time average of $P_{SE}(t)$ it is more convenient to use the mass eigenstate basis. Let us denote

$$\alpha_e(t) = s_1 \mathrm{e}^{\mathrm{i}\omega_1 t} + s_2 \mathrm{e}^{\mathrm{i}\omega_2 t} + s_3 \mathrm{e}^{\mathrm{i}\omega_3 t}, \tag{11}$$

$$\beta_e(t) = t_1 \mathrm{e}^{\mathrm{i}\omega_1 t} + t_2 \mathrm{e}^{\mathrm{i}\omega_2 t} + t_3 \mathrm{e}^{\mathrm{i}\omega_3 t}, \tag{12}$$

$$\gamma_e(t) = u_1 \mathrm{e}^{\mathrm{i}\omega_1 t} + u_2 \mathrm{e}^{\mathrm{i}\omega_2 t} + u_3 \mathrm{e}^{\mathrm{i}\omega_3 t}, \tag{13}$$

where s_i, t_i, u_i are independent of time. Then we have

$$\alpha_e\alpha_e^* = s_1 s_1^* + s_2 s_2^* + s_3 s_3^* + \text{cross terms}, \tag{14}$$

$$\begin{aligned}\alpha_e\beta_e^* &= s_1 t_1^* + s_2 t_2^* + s_3 t_3^* + \text{cross terms}\\ &= (s_{1R}t_{1R} + s_{1I}t_{1I}) + \mathrm{i}(s_{1I}t_{1R} - s_{1R}t_{1I})\\ &\quad + (s_{2R}t_{2R} + s_{2I}t_{2I}) + \mathrm{i}(s_{2I}t_{2R} - s_{2R}t_{2I})\\ &\quad + (s_{3R}t_{3R} + s_{3I}t_{3I}) + \mathrm{i}(s_{3I}t_{3R} - s_{3R}t_{3I})\\ &\quad + \text{cross terms}\\ &\equiv R_{\alpha\beta} + \mathrm{i}I_{\alpha\beta} + \text{cross terms},\end{aligned} \tag{15}$$

where

$$\begin{aligned}R_{\alpha\beta} &= (s_{1R}t_{1R} + s_{1I}t_{1I}) + (s_{2R}t_{2R} + s_{2I}t_{2I})\\ &\quad + (s_{3R}t_{3R} + s_{3I}t_{3I}),\end{aligned} \tag{16}$$

$$\begin{aligned}I_{\alpha\beta} &= (s_{1I}t_{1R} - s_{1R}t_{1I}) + (s_{2I}t_{2R} - s_{2R}t_{2I})\\ &\quad + (s_{3I}t_{3R} - s_{3R}t_{3I}).\end{aligned} \tag{17}$$

The cross terms cancel out upon time averaging.

It is convenient to express the amplitudes (a_e, a_μ, a_τ) in the weak eigenstate basis in terms of those in the mass eigenstate basis, (a_1, a_2, a_3),

$$\begin{aligned}a_e(t) &= U_{11}a_1(t) + U_{12}a_2(t) + U_{13}a_3(t),\\ a_\mu(t) &= U_{21}a_1(t) + U_{22}a_2(t) + U_{23}a_3(t),\\ a_\tau(t) &= U_{31}a_1(t) + U_{32}a_2(t) + U_{33}a_3(t).\end{aligned} \tag{18}$$

Averaging over time, we obtain

$$X_e^2 = \langle a_e a_e^*\rangle = U_{11}^2|a_1|^2 + U_{12}^2|a_2|^2 + U_{13}^2|a_3|^2, \quad \ldots. \tag{19}$$

We solve this equation for $|a_i|^2$. Then we can express $\langle a_e a_\mu^*\rangle$ in terms of $|a_i|^2$. Let us denote

$$\begin{aligned}\langle a_e a_\mu^*\rangle &= U_{11}U_{21}a_1a_1^* + U_{12}U_{22}a_2a_2^* + U_{13}U_{23}a_3a_3^*\\ &\equiv X_{e\mu} + \mathrm{i}Y_{e\mu}.\end{aligned} \tag{20}$$

We notice that the phases of a_i become irrelevant upon time-averaging. Now we get the time average

$$\begin{aligned}&\langle[a_e\alpha_e a_\mu^*\beta_e^* + \text{c.c.}]\rangle\\ &= \left[(R_{\alpha\beta} + \mathrm{i}I_{\alpha\beta})(X_{e\mu} + \mathrm{i}Y_{e\mu}) + \text{c.c.}\right]\\ &= 2(R_{\alpha\beta}X_{e\mu} - I_{\alpha\beta}Y_{e\mu}).\end{aligned} \tag{21}$$

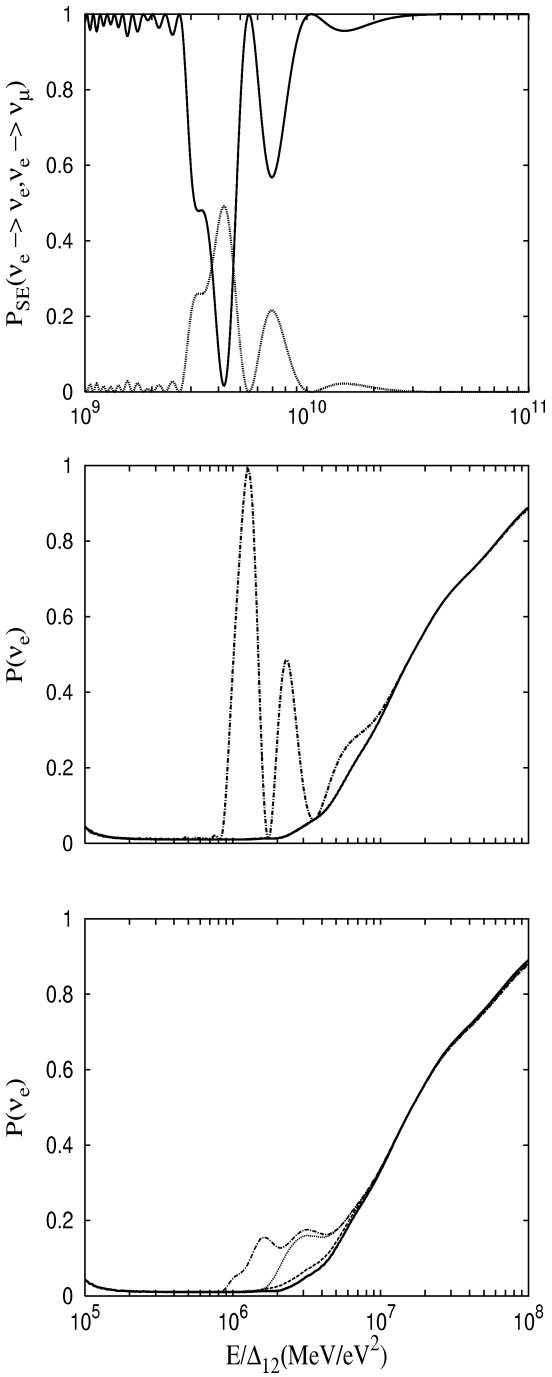

Fig. 1. Comparison of earth regenerated solar neutrino fluxes: (top) Fig. 1 of Ohlsson Ref. [66]; (middle) Fig. 3(d) of Baltz and Weneser (1987), Ref. [54]; (bottom) Fig. 5(d) of Ref. [54].

Similarly working on other terms and collecting all terms, we obtain the time averaged probability of a solar neutrino to emerge as an electron neutrino after passing the earth,

$$\begin{aligned}\langle P_{SE}\rangle \;=\; & |a_e|^2|\alpha_e|^2 + |a_\mu|^2|\beta_e|^2 + |a_\tau|^2|\gamma_e|^2 \\ & + 2(R_{\alpha\beta}X_{e\mu} - I_{\alpha\beta}Y_{e\mu} + R_{\beta\gamma}X_{\mu\tau} \\ & - I_{\beta\gamma}Y_{\mu\tau} + R_{\gamma\alpha}X_{\tau e} - I_{\gamma\alpha}Y_{\tau e}). \qquad (22)\end{aligned}$$

In order to check our algorithm we reproduced some figures published in the literatures [57,67] in the limit $\theta_{13} \to 0$ (see Fig. 1). Our figures agree with the results as illustrated in Fig. 4 of [57] in the range $E < 10^8$. Our figures completely agree with the results obtained by using the time averaged $P_E(\nu_2 \to \nu_e)$ in Eq. (1) of [67].

4. Survival probabilities of a solar neutrino with non-zero θ_{13}

We consider the effects of non-zero θ_{13} on the electron neutrino survival probabilities of an electron neutrino created at the center of the Sun as a function of $E' \equiv E/\Delta_{12}$ in MeV/eV^2. We illustrate two cases in Fig. 2. In Fig. 2(a) we consider the Small Mixing Angle (SMA) case using the set of parameter values ($\sin^2(2\theta_{12}) = 4.40 \times 10^{-3}$, $\Delta_{12} = 6.31 \times 10^{-6}$ eV^2). It consists of 3 plots corresponding to $\theta_{13} = 5^\circ,\ 22.5^\circ,\ 45^\circ$. Fig. 2(b) corresponds to the Large Mixing Angle (LMA) case and ($\sin^2(2\theta_{12}) = 0.76$, $\Delta_{12} = 1.8 \times 10^{-5}$ eV^2) was used. The upper limit of solar neutrino energy, 20 MeV is indicated by the downward arrow. Each plot contains a curve for raw solar neutrino flux and five curves marked by Sm corresponding to five neutrino paths with nadir angles $\eta = (m/10)(\pi/2)$.

Neutrinos undergo resonance conspicuously in those regions where the curves oscillate widely away from the raw curve. We notice that for nonzero values of the (1-3) mixing angle θ_{13} double resonances occur, one in the range $10^6 < E' < 10^7$ and the other in $10^8 < E' < 10^{10}$. The resonance in the low range is caused by non-zero θ_{12} and its amplitude grows larger for large θ_{12}. The resonance in the high range is due to non-zero θ_{13} and it is enhanced for large θ_{13}. The resonances occur for all nadir angles with almost equal strengths. It is noteworthy that for low energy solar

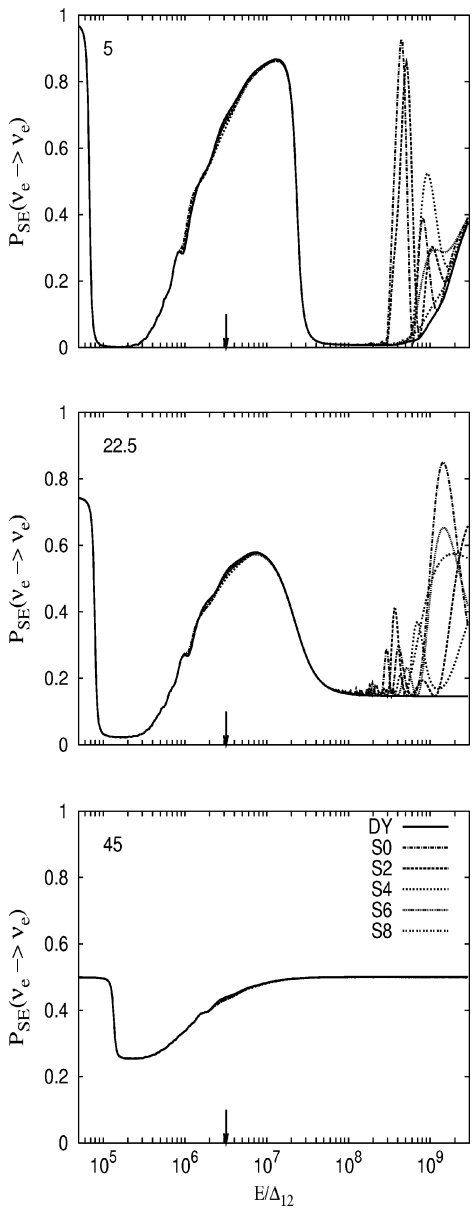

(a)

Fig. 2(a). Earth regenerated solar neutrino fluxes (SMA case). The solid curve (DY) is for raw flux and the others marked by Sm are for the paths with the nadir angles $\eta = (m/10)(\pi/2)$. All solar neutrinos are created at the center of the Sun. Downward arrows mark the 20 MeV upper limit of E_ν. We used the mixing parameters: $\Delta m^2_{23} = 2.2 \times 10^{-3}$ eV^2, $\theta_{23} = 43.5°$. The values of θ_{13} are inscribed in the plots. For the SMA case: $\Delta m^2_{12} = 6.31 \times 10^{-6}$ eV^2, $\sin^2(2\theta_{12}) = 4.40 \times 10^{-3}$. For the LMA case: $\Delta m^2_{12} = 1.8 \times 10^{-5}$ eV^2, $\sin^2(2\theta_{12}) = 0.76$.

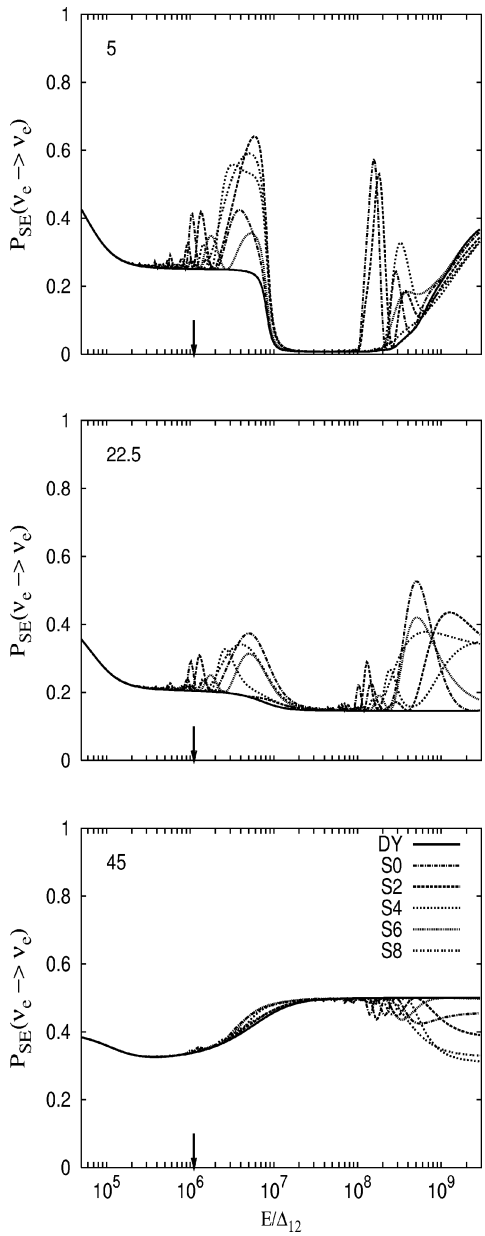

(b)

Fig. 2(b). Earth regenerated solar neutrino fluxes (LMA case).

neutrinos the earth effect is larger for smaller values of the nadir angle.

Fig. 2(a) reveals that in the SMA case the earth effect for low energy solar neutrinos ($E < 20$ MeV)

is minor for all values of θ_{13}. Fig. 2(b) exhibits that in the LMA case the earth effect is non-trivial for some high energy ^{8}B and *hep* solar neutrinos. It is most significant for small values of θ_{13} and diminishes for large θ_{13}.

Since it costs a lot of computation to trace neutrinos for each nadir angle we need to make a strategy for handling the angular effect. We exploit that for a given set of parameters, the neutrino wavefunctions are smooth functions of the nadir angle η. We thus compute at a finite number of angles and then build an interpolation function. For the nadir angle, we choose $\cos(\eta)$ as the sampling function. Thus we sample more frequently near $\eta = 0$ and scarcely near $\eta = \pi/2$. We selected 25 nadir angles between 0 and $\pi/2$. For low energy solar neutrinos the earth effect diminishes for $\eta > \eta_c = 0.5779$, the nadir angle grazing the boundary between the core and the mantle. Thus our sampling strategy works fine. An interpolation function made from these 25 η values will be fairly accurate to use.

We can now compute the states of pure neutrinos, $\Psi_e(t)$, $\Psi_\mu(t)$, $\Psi_\tau(t)$ at discrete energies and nadir angles selected according to the importance sampling functions. In our previous works on solar neutrino flux [52], we selected energy sampling points according to the convolution of the neutrino energy distribution functions as they are created in the solar core and the detector cross sections. In the present work we added 7 more energy sample points in the interval $0.23 \leqslant E \leqslant 0.737$ MeV to account for the CNO neutrinos more faithfully.

5. Long term averages: daily, monthly and yearly averages

We have compiled a large amount of raw solar neutrino fluxes for a reasonably large area in the parameter space, $(\Delta_{12}, \sin^2(2\theta_{12}))$ for selected values of θ_{13}, using the method described in [52]. Our results were partially reported without the earth effect in [53]. The results of our computations in the $\theta_{13} \to 0$ limit have been carefully checked against the results obtained with the analytic approximation formula such as the Petcov's improved formula [18]. We agree with their results in the range of creation positions where their results are reliable as they claimed, in the sense that their formula give the flux values averaged over the creation positions whereas ours give the fluxes created at exact positions as illustrated in Fig. 5 of Ref. [49]. We also compared the survival probabilities of a neutrino created at the center of the Sun in the range of E' for various sets of mixing parameters. The agreement is to one part in 1000 in the worst case. Since our results are computed numerically we have equally accurate fluxes beyond their claimed range. For three neutrino cases, analytic formula for survival probabilities for simple densities have been derived only recently [49–51]. We have already confirmed that our subroutines reproduce the same results as those given in [69].

Next we compute seasonal variations of daily averages. The nadir angle η of a neutrino path can be written [67] as a function of the date of year τ_d from the winter solstice, the time of day τ_h from the midnight and the latitude λ as follows,

$$\cos(\eta) = \cos(\lambda)\cos(\tau_h)\cos(\delta_S) - \sin(\lambda)\sin(\delta_S), \quad (23)$$

where the Sun declination is given by $\sin(\delta_S) = -\sin(i_E)\cos(\tau_d)$ and $i_E = 0.4091$ is the earth inclination.

We illustrate the survival probabilities for two interesting parameter sets in Fig. 3. The average was taken over every 12 minutes for 24 hours on three days, the winter solstice (dotted), the vernal equinox (dash-dotted) and the summer solstice (dashed). The raw solar neutrino flux is plotted with the solid curve. The latitude of Gran Sasso was used. The downward arrows mark the point of $E = 20$ MeV, the upper bound of the solar neutrino energy. Each set consists of 4 plots corresponding to $\theta_{13} = 0^\circ,\ 1.5^\circ,\ 15^\circ,\ 22.5^\circ$. As we notice from Fig. 3(a), in the small mixing angle case the electron neutrino survival probability is almost unaffected by the earth effect as in the two neutrino case, regardless of θ_{13}. Fig. 3(b) shows that in the large mixing angle case (we used $\sin^2(2\theta_{12}) = 0.63$, $\Delta_{12} = 1.3 \times 10^{-5}$ eV^2 in Fig. 3(b)) the earth effect is non-negligible for high energy neutrinos. The effect is maximal for $\theta_{13} = 0$ and diminishes as θ_{13} is increased.

We are now equipped with all the routines that are needed to compute average fluxes in an extended period of time. Since we used the importance sampling method for selecting reasonably large number of creation positions and energies to set up an interpolation function that is particularly good in the important

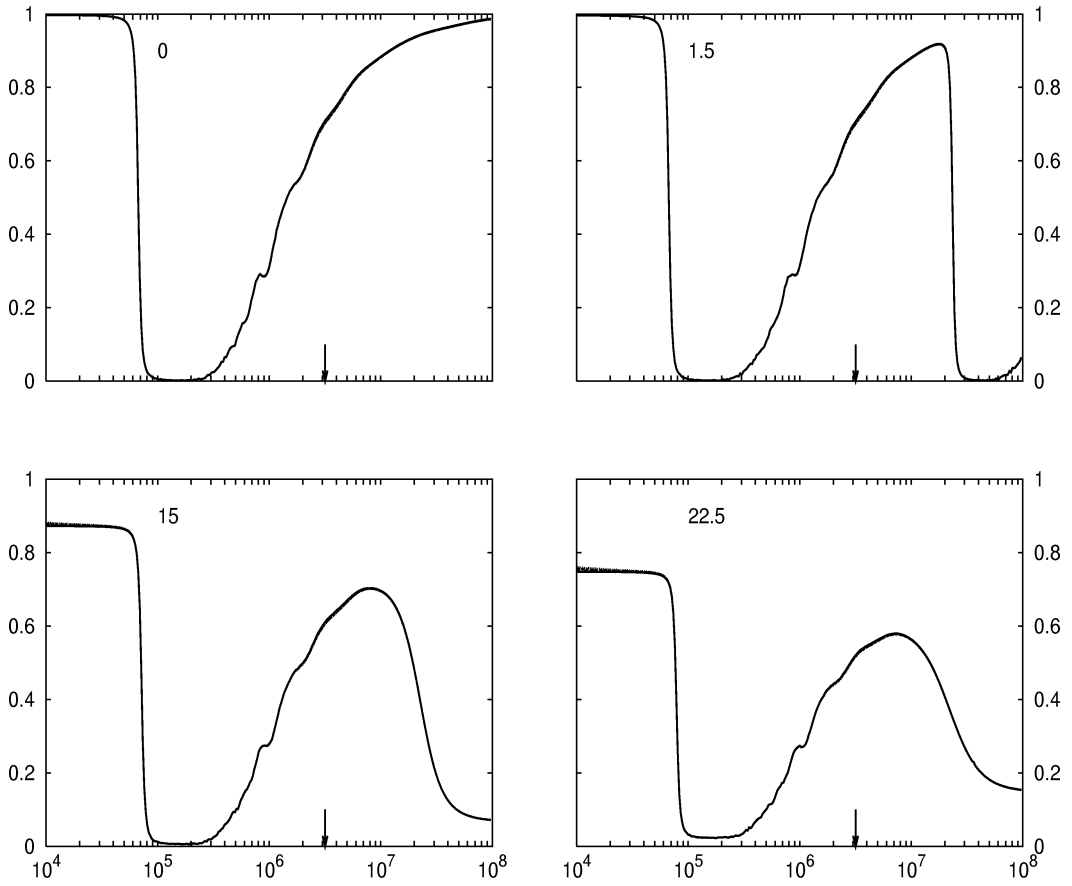

Fig. 3(a). Daily averages of solar neutrino fluxes (SMA case). Solid curves are for raw flux, dotted ones for earth regenerated flux on the winter solstice, dashed ones on the summer solstice, dash-dotted ones on the equinox. All solar neutrinos are created at the center of the Sun. Downward arrows mark the 20 MeV upper limit of E_ν. We used the mixing parameters: $\Delta m^2_{23} = 2.2 \times 10^{-3}$ eV^2, $\theta_{23} = 43.5°$. The values of θ_{13} are inscribed in the plots. For the SMA case: $\Delta m^2_{12} = 6.31 \times 10^{-6}$ eV^2, $\sin^2(2\theta_{12}) = 4.36 \times 10^{-3}$. For the LMA case: $\Delta m^2_{12} = 1.3 \times 10^{-5}$ eV^2, $\sin^2(2\theta_{12}) = 0.63$.

ranges, we can reproduce the fluxes with high accuracy for creation position and energy values within the those ranges.

We have computed a large number of states of pure neutrinos, $\Psi_e(t)$, $\Psi_\mu(t)$, $\Psi_\tau(t)$ at 100 discrete energies and 25 nadir angles. We used 40 energy sample points for *pp* neutrinos in the interval $0.23 < E < 0.737$ MeV similarly picked as in [52,53] and the same 60 points as used in [52,53] in the interval $0.737 < E < 19$ MeV for boron and CNO neutrinos, for the same set of parameters $(\Delta_{12}, \sin^2(2\theta_{12}), \theta_{13})$. We handpicked three important energy points, $E = 0.384,\ 0.862,\ 1.442$ MeV for Be neutrinos and pep neutrinos respectively. Each integration of the neutrino evolution equations in the earth takes only a modest amount of computing time but the huge number of integrations requires a large amount of total computing time. We again have to resort to a parallel supercomputer. The parallelization can be done using the same method as described in [52].

Using these data we can compute the earth regeneration effect on the survival probability of an incident solar neutrino at any energy and any nadir angle for a selected set of mixing parameters. In this way we can compute the earth regenerated solar neutrino fluxes for a large region of the mixing parameter space with a

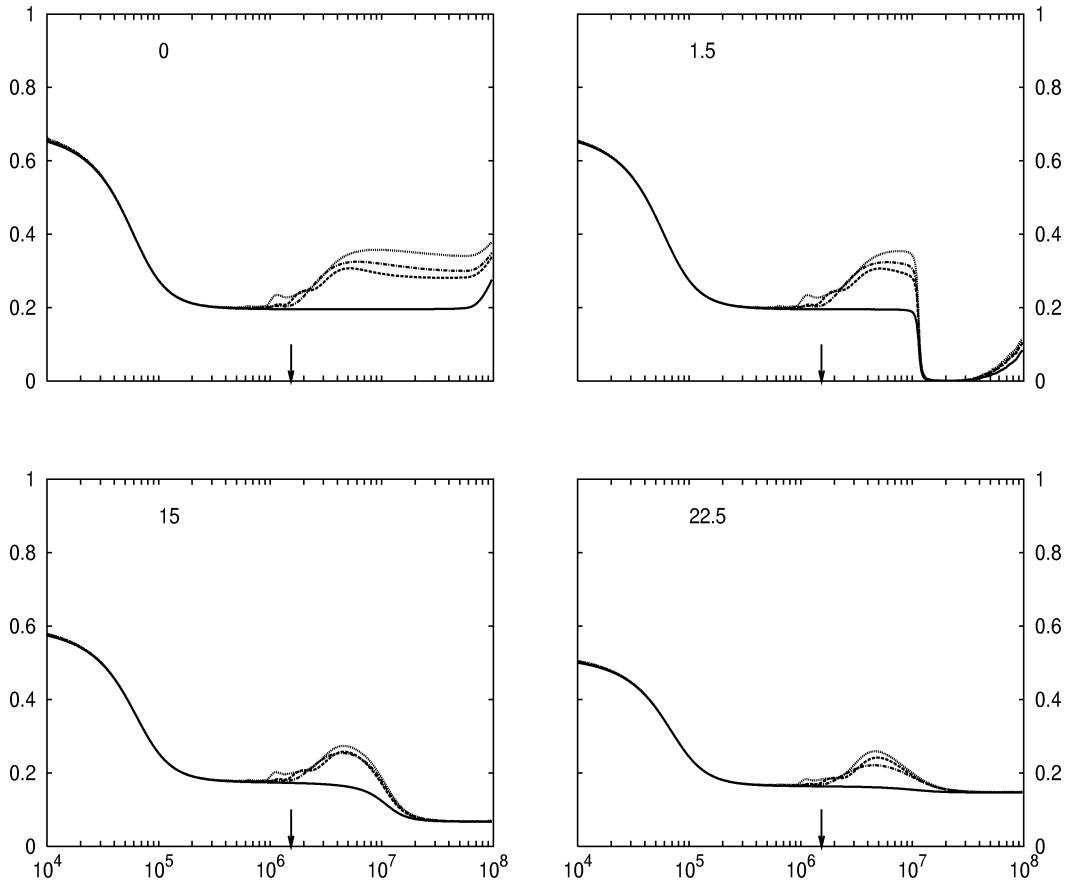

Fig. 3(b). Daily averages of solar neutrino fluxes (LMA case).

modest number of energy samplings to yield an accurate estimate of event rates.

Some cautions are needed for setting up an interpolation function for creation positions and energies. We illustrate the solar neutrino survival probability as a function of creation position in Fig. 4, where we see a very sharply rising curve. We see a sharply dropping curve in Fig. 2(a). Since we are using only a finite number of samples with different spacings we will encounter a sticky situation when the curves happen to turn sharply in the region where the sample spacing is wide. The popular cubic spline interpolation fails badly in this situation. One needs to use the exponential spline [71]. We used the FITPACK subroutines available in the GAMS library [74]. As Fig. 4 shows the interpolated curve is as good as the original one.

6. Sample contour plots

We illustrate sample iso-SNU(FLUX) contour plots in the plane, $(\sin^2(2\theta_{12}) - \Delta_{12})$, for a set of mixing parameters, $\Delta_{23} = 2.2 \times 10^{-3}$ eV^2, and $\theta_{23} = 43.5°$, $\theta_{13} = 1.5°,\ 15°$ in Figs. 5–8. We made separate plots for each experiment [10–13] with appropriate latitude λ. For a given set of $(\sin^2(2\theta_{12}), \Delta_{12})$ we had generated solar neutrinos according to the SSM model [1, 2]. In order to compute the raw solar neutrino fluxes we used 36 creation positions and 60 energy samples for pp neutrino and 60 creation positions and $60 + 7$ energy samples for others. For the same set of mixing parameters $(\sin^2(2\theta_{12}), \Delta_{12})$ we had computed the states of three pure neutrinos, $\Psi_e(t)$, $\Psi_\mu(t)$, $\Psi_\tau(t)$ at 100 discrete energies and 25 nadir angles optimally

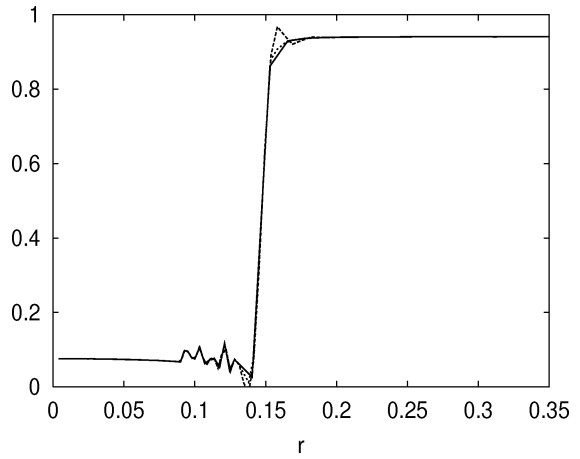

Fig. 4. Survival probability of a solar neutrino as a function of creation position. Original data are marked by the solid curve, the cubic spline fit by the dashed and the exponential fit by the dotted.

selected as explained in Section 4. For each solar neutrino created at position r with energy E we perform a sequence of time averaging operations leading to Eq. (22). In this way we build an interpolation function for $\langle P_{SE}(r, E, \eta)\rangle$ as a function of creation position r, energy E and nadir angle η. We integrate the fluxes over the creation positions according to the relevant creation probability distribution functions and then build an interpolation function for $\langle P_{SE}(E, \eta)\rangle$ as a function of the energy and nadir angle. We can now take seasonal and yearly averages of this flux to get $\langle P_{SE}(E)\rangle$, which involves integration over η with a definite latitude λ. Finally we take a convolution of $\langle P_{SE}(E)\rangle$ with the absorption cross sections $\sigma(E)$ to get the yearly average of event rate for a particular experiment.

For those experiments like Super-Kamiokande and SNO, we need to take into account of electron recoil spectrum [75–80]. For the Super-Kamiokande experiment with the threshold recoil energy $T_{th} = 5$ MeV we use the following formula for convolution,

$$R = f_B \int_{5.5}^{16.5} \mathrm{d}E \int_{5}^{T_M} \mathrm{d}T \int_{0}^{T_M} r(T, T')\phi_B(E) \times \left[\frac{\mathrm{d}\sigma_e}{\mathrm{d}T'}\langle P_{SE}(E)\rangle + \frac{\mathrm{d}\sigma_X}{\mathrm{d}T'}\big(1 - \langle P_{SE}(E)\rangle\big)\right]\mathrm{d}T', \quad (24)$$

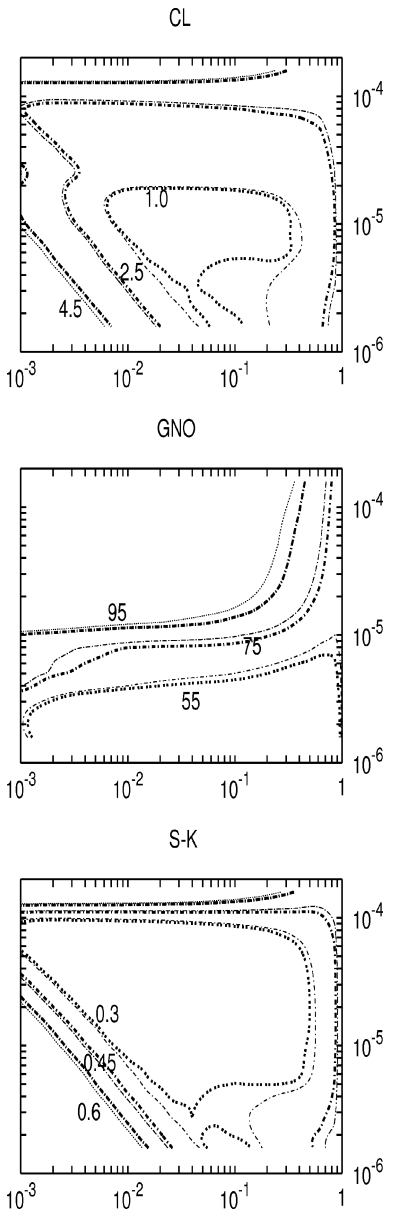

Fig. 5. The seasonal variations of iso-SNU contours for solar neutrinos with the Cl, Ga and H_2O detectors ($\theta_{13} = 1.5°$). Contours are for SNU values (1.0, 2.5, 4, 5) [Cl], (55, 75, 95) [Ga]. For the Super-Kamiokande [H_2O] detector the contours are for ratios with respect to the SSM expectation (0.3, 0.45, 0.6). The thick curves are for the winter period and the thin curves are for the summer period, respectively. In each plot the vertical axis refers to Δ_{12} in eV^2 and the horizontal axis to $\sin^2(2\theta_{12})$. We used $\Delta_{23} = 2.2 \times 10^{-3}$ eV^2, $\theta_{23} = 43.5°$, $\theta_{13} = 1.5°$.

where E is the neutrino energy in MeV, T is the measured kinetic energy of a recoil electron and T' the true energy. $\phi_B(E)$ is the normalized energy spectrum of the boron neutrino and f_B is its total flux. The maximum kinetic energy of a recoil electron is given by $T_M = 2E^2/(m_e + 2E)$. The measured electron kinetic energies are assumed to have the Gaussian distribution function,

$$r(T, T') = \frac{1}{\sqrt{2\pi}s} \exp\bigl(-(T - T')^2/2s^2\bigr). \tag{25}$$

We use $s = s_0\sqrt{E}$ with $s_0 = 0.47$ MeV as employed in literature. For the differential cross sections, $\mathrm{d}\sigma_e/\mathrm{d}T'$ for $(\nu_e + e)$ and $\mathrm{d}\sigma_X/\mathrm{d}T'$ for $(\nu_X + e)$, we use the formula with radiative corrections given in [81]. In Eq. (24) the same $\mathrm{d}\sigma_X/\mathrm{d}T'$ is used for both muon and tau neutrinos because of unsettled parameters in the Higgs sector.

In order to make iso-SNU(FLUX) contour plots, we used a 16×21 logarithmic mesh in the $(\sin^2(2\theta_{12}) - \Delta_{12})$ plane in the range $0.001 \leqslant \sin^2(2\theta_{12}) \leqslant 1$ and $1.58 \times 10^{-6} \leqslant \Delta_{12} \leqslant 1.58 \times 10^{-4}$ eV^2. We padded two extra values, $(0.85, 0.97)$, for $\sin^2(2\theta_{12})$ in order to examine the large θ_{12} region more carefully.

We plot the seasonal variations of iso-SNU contours in Fig. 5 ($\theta_{13} = 1.5°$) and in Fig. 6 ($\theta_{13} = 15°$). We compared the winter average taken over the two month period after the winter solstice and the summer average taken over the two month period before the summer solstice. As expected from previous figures, contours in the SMA region are almost intact but in the small $\Delta_{12} < 10^{-5}$ eV^2 and large $\sin^2(2\theta_{12}) > 0.1$ region the contours are distorted significantly by the earth effect. The Cl and water detectors are somewhat insensitive in most regions of the parameter space but they are sensitive in the lower-right region. The Ga detector is more sensitive to the seasonal changes than the other two.

In Fig. 7 we plot the θ_{13} dependence of the annual averages. The differences are small in the SMA region in general. The Ga detector shows large differences between the two values of θ_{13}. Since it is also sensitive to the season changes the Ga data can be used for determining the mixing parameters independently from the other experiments.

In Fig. 8 we plot the annual averages of day-night differences in the Super-Kamiokande detector. The D/N difference is defined as $\delta = 2(N - D)/(N +$

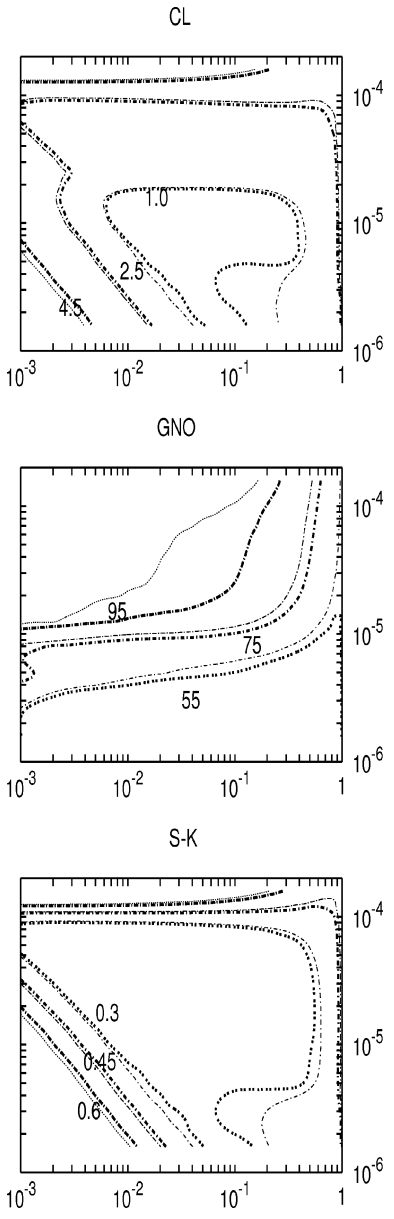

Fig. 6. The seasonal variations of iso-SNU contours for solar neutrinos with the Cl, Ga and H_2O detectors ($\theta_{13} = 15°$). The same as Fig. 5 with $\theta_{13} = 15°$. In order to show how the contours change, we kept the positions of labels the same as in Fig. 5.

D), which is independent of the total flux of the boron neutrino. The contours are very sensitive for $\delta < 0.05$. Slight change of δ can sway the contour wildly. This high sensitivity can be used to determine

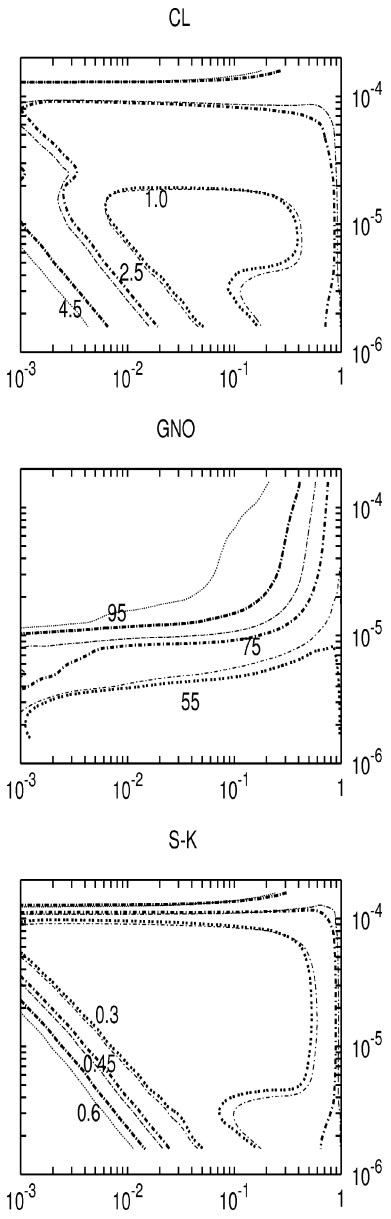

Fig. 7. The θ_{13} dependence of iso-SNU contours for solar neutrinos with the Cl, Ga and H_2O detectors. Contours are for SNU values $(1.0, 2.5, 4, 5)$ [Cl], and $(55, 75, 95)$ [Ga]. For the Super-Kamiokande [H_2O] detector the contours are for ratios with respect to the SSM expectation $(0.30, 0.45, 0.60)$. The thick curves are for $\theta_{13} = 1.5^\circ$ and the thin curves are for $\theta_{13} = 15^\circ$, respectively. In all cases we plotted the annual average values. In each plot the vertical axis refers to Δ_{12} in eV^2 and the horizontal axis to $\sin^2(2\theta_{12})$. We used $\Delta_{23} = 2.2 \times 10^{-3}$ eV^2, $\theta_{23} = 43.5^\circ$.

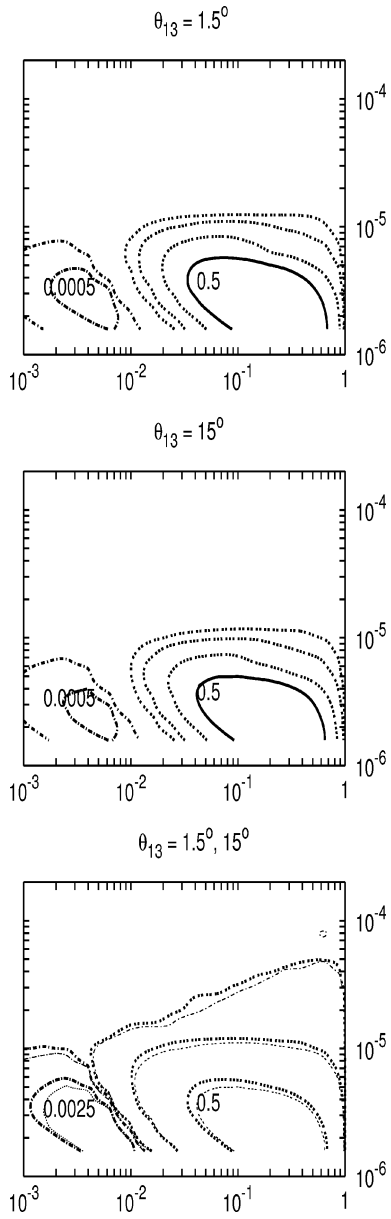

Fig. 8. D/N differences for the Super-Kamiokande H_2O detector. Contours are for $\delta = 2(N - D)/(N + D)$ values $(0.5, 0.25, 0.1, 0.05, 0.005, 0.0005)$ in the two upper figures and $(0.5, 0.065, 0.01, 0.007, 0.0025)$ in the last figure. In the last figure the thick curves are for $\theta_{13} = 1.5^\circ$ and the thin curves are for $\theta_{13} = 15^\circ$, respectively. In all cases we plotted the annual average values. In each plot the vertical axis refers to Δ_{12} in eV^2 and the horizontal axis to $\sin^2(2\theta_{12})$. We used $\Delta_{23} = 2.2 \times 10^{-3}$ eV^2, $\theta_{23} = 43.5^\circ$.

the (1-2) mixing parameters. But a high precision measurement of δ is required to pinpoint Δ_{12} and θ_{12}. Our numerical analysis also seems to need further refinement, namely more sample points, in the region $(0.001 < \sin^2(2\theta_{12}) < 0.01)$. The contours in this range passes both the SMA and LMA regions.

7. Summary and conclusion

We introduced an integrated algorithm to deal with the earth regeneration effect of solar neutrinos with all three active neutrinos considered. Main ingredients of the algorithm are the time averaging algorithm with the use of mass eigenstates, the strategy for sampling energy and nadir angle, and the interpolation algorithm. Our algorithm is useful for full scale investigation of the earth effect.

We illustrated that the earth effect on low energy solar neutrinos causes large variations in the survival probabilities for large mixing angles θ_{12} at a given value of θ_{13}. But it is maximal for small values of θ_{13} and diminishes for large values ($\sim 45^\circ$) at a given value of θ_{12}. The nadir angle dependence is sensitive to the value of E'. As far as low energy solar neutrinos are concerned we notice that the earth effect is more pronounced for smaller nadir angles.

We have shown that for large values of θ_{13}, the earth effect is significant for high energy accelerator or atmospheric neutrinos ($E' > 10^9$) and it can be large at any nadir angle.

We made various sample plots of iso-SNU contours. From these plots, we showed the possibility that combination of the seasonal variations of Ga data and the D/N difference of water data can lead to determination of the three mixing parameters, Δ_{12}, θ_{12}, θ_{13} decisively.

References

[1] J.N. Bahcall, M.H. Pinsonneault, Rev. Mod. Phys. 67 (1995) 781.
[2] J.N. Bahcall, S. Basu, M.H. Pinsonneault, Phys. Lett. B 433 (1998) 1.
[3] S. Turck-Chièze, I. Lopes, Astrophys. J. 408 (1993) 347.
[4] R. Davis Jr., D.S. Harmer, K.C. Hoffman, Phys. Rev. Lett. 20 (1968) 1205.
[5] B. Pontecorvo, Zh. Eksp. Teor. Fiz. 53 (1967) 1717; Sov. Phys. JETP 26 (1968) 984.
[6] M. Gell-Mann, P. Ramond, R. Slansky, Supergravity, in: F. van Nieuwenhuizen, D. Freeman (Eds.), North-Holland, Amsterdam, 1979, p. 315.
[7] S.M. Bilenky, B. Pontecorvo, Phys. Rep. 41 (1978) 225.
[8] V. Gribov, B. Pontecorvo, Phys. Lett. B 28 (1969) 493.
[9] J.N. Bahcall, S. Frautschi, Phys. Lett. B 29 (1969) 623.
[10] Homestake Collaboration, B.T. Cleveland et al., Nucl. Phys. (Proc. Suppl.) B 38 (1995) 47; Astrophys. J. 496 (1998) 505.
[11] GALLEX Collaboration, P. Anselmann et al., Phys. Lett. B 342 (1995) 440;
W. Hampel et al., Phys. Lett. B 388 (1996) 384; Phys. Lett. B 447 (1999) 127.
[12] SAGE Collaboration, A.I. Abazov et al., Phys. Rev. Lett. 67 (1991) 3332;
J.N. Abdurashitov et al., Phys. Lett. B 328 (1994) 234;
J.N. Abdurashitov et al., astro-ph/9907131.
[13] Super-Kamiokande Collaboration, Y. Fukuda et al., Phys. Rev. Lett. 77 (1996) 1683;
Y. Suzuki et al., in Neutrino '98;
Y. Fukuda et al., Phys. Rev. Lett. 82 (1999) 1810.
[14] L. Wolfenstein, Phys. Rev. D 17 (1978) 2369.
[15] S.P. Mikheyev, A.Yu. Smirnov, Yad. Fiz. 42 (1985) 1441; Sov. H. Nucl. Phys. 42 (1985) 913.
[16] S. Parke, Phys. Rev. Lett. 57 (1986) 1275.
[17] S. Toshev, Phys. Lett. B 196 (1987) 170.
[18] S.T. Petcov, Phys. Lett. B 200 (1988) 373;
P.I. Krastev, S.T. Petcov, Phys. Lett. B 207 (1988) 64;
S.T. Petcov, Phys. Lett. B 406 (1997) 355.
[19] M. Bruggen, W.C. Haxton, Y.-Z. Qian, Phys. Rev. D 51 (1995) 4028.
[20] A.B. Balantekin, J.F. Beacom, J.M. Fetter, Phys. Lett. B 427 (1998) 317.
[21] G. Fiorentini, M. Lissia, G. Mezzorani, M. Moretti, D. Vignaud, Phys. Rev. D 49 (1994) 6298.
[22] N. Hata, P. Langacker, Phys. Rev. D 52 (1995) 420; Phys. Rev. D 56 (1997) 6107.
[23] J.N. Bahcall, P.I. Krastev, A.Yu. Smirnov, Phys. Rev. D 58 (1998) 096016.
[24] Super-Kamiokande Collaboration, Y. Fukuda, Phys. Lett. B 433 (1998) 9; Phys. Lett. B 436 (1998) 33; Phys. Rev. Lett. 81 (1998) 1562.
[25] R.P. Thun, S. McKee, Phys. Lett. B 439 (1998) 123.
[26] V. Barger, K. Whisnant, Phys. Rev. D 59 (1999) 093007.
[27] G.L. Fogli, E. Lisi, A. Marrone, G. Scioscia, Phys. Rev. D 59 (1999) 033001;
G.L. Fogli, E. Lisi, D. Montanino, G. Scioscia, Phys. Rev. D 55 (1997) 4385.
[28] O.L.G. Peres, A.Yu. Smirnov, Phys. Lett. B 456 (1999) 204.
[29] J.T. Peltoniemi, D. Tommasini, J.W.F. Valle, Phys. Lett. B 298 (1993) 383.
[30] E. Ma, P. Roy, Phys. Rev. D 52 (1995) 4780.
[31] E.J. Chun, A.S. Joshipura, A.Yu. Smirnov, Phys. Lett. B 357 (1995) 608.
[32] S.M. Bilenky, C. Giunti, W. Grimus, Eur. Phys. J. C 1 (1998) 247.
[33] D. Dooling, C. Giunti, K. Kang, C.W. Kim, Phys. Rev. D 61 (2000) 073011.

[34] C. Giunti, M.C. Gonzalez-Garcia, C. Pĕna-Garay, Rev. D 62 (2000) 013005.
[35] T.K. Kuo, J. Pantaleone, Phys. Rev. Lett. 57 (1986) 1805; Rev. Mod. Phys. 61 (1989) 937.
[36] S.P. Mikheyev, A.Yu. Smirnov, Phys. Lett. B 200 (1988) 560.
[37] X. Shi, D.N. Schramm, Phys. Lett. B 283 (1992) 305.
[38] A. Baldini, G.F. Giudice, Phys. Lett. B 186 (1987) 211.
[39] C.W. Kim, W.K. Sze, Phys. Rev. D 35 (1987) 1404.
[40] S.T. Petcov, S. Toshev, Phys. Lett. B 187 (1987) 120.
[41] H.W. Zaglauer, K.H. Schwarzer, Z. Phys. C 40 (1988) 273.
[42] A.S. Joshipura, P.I. Krastev, Phys. Rev. D 50 (1994) 3484.
[43] D. Harley, T.K. Kuo, J. Pantaleone, Phys. Rev. D 47 (1993) 4059.
[44] G.L. Fogli, E. Lisi, D. Montanino, Phys. Rev. D 49 (1994) 3626; Astropart. Phys. 4 (1995) 177; Phys. Rev. D 54 (1996) 2048.
[45] G.L. Fogli, E. Lisi, D. Montanino, A. Palazzo, hep-ph/9912231.
[46] T. Sakai, O. Inagaki, T. Teshima, Int. J. Mod. Phys. A 12 (1999) 1953.
[47] R. Barbieri, L.J. Hall, D. Smith, A. Strumia, N. Weiner, hep-ph/9807235, JHEP 9812:017 (1998).
[48] M.C. Gonzalez-Garcia, P.C. de Holanda, C. Pĕna-Garay, J.W.F. Valle, Nucl. Phys. B 573 (2000) 3.
[49] E. Torrente Lujan, Phys. Rev. D 53 (1996) 4030.
[50] T. Ohlsson, H. Snellman, hep-ph/9910546.
[51] P. Osland, T.T. Wu, hep-ph/9912540.
[52] J.S. Kim, Y.S. Chae, J.D. Kim, Comput. Phys. Comm. 120 (1999) 41.
[53] J.S. Kim, C.W. Kim, hep-ph/9909428.
[54] F.D. Stacey, Physics of the Earth, 2nd edn., Wiley, New York, 1977.
[55] J. Bouchez, M. Cribier, W. Hampel, J. Rich, D. Vignaud, Z. Phys. C 32 (1986) 499; Phys. Lett. B 182 (1986) 89.
[56] E.D. Carlson, Phys. Rev. D 34 (1986) 1454.
[57] A.J. Baltz, J. Weneser, Phys. Rev. D 35 (1987) 528; Phys. Rev. D 37 (1988) 3364; Phys. Rev. D 50 (1994) 5971.
[58] A. Dar, A. Mann, Y. Melina, D. Zajfman, Phys. Rev. D 35 (1987) 3607.
[59] M.L. Cherry, K. Lande, Phys. Rev. D 36 (1987) 3571.
[60] S. Hiroi, H. Sakuma, T. Yanagida, M. Yoshimura, Phys. Lett. B 198 (1987) 403.
[61] G. Auriemma, M. Felcini, P. Lipari, J.L. Stone, Phys. Rev. D 37 (1988) 665.
[62] S.P. Mikheyev, A.Yu. Smirnov, in: O. Fackler, J. Trân Thanh Vân (Eds.), Moriond'87, Proc. of 7th Moriond Workshop on New and Exotic Phenomena, Les Arcs, France, Frontières, Paris, 1987, p. 405.
[63] Kamiokande Collaboration, K.S. Hirata et al., Phys. Rev. Lett. 65 (1990) 1301.
[64] J.M. LoSecco, Phys. Rev. D 47 (1993) 2032.
[65] A.J. Baltz, J. Weneser, Phys. Rev. D 50 (1994) 5971.
[66] Q.Y. Liu, M. Maris, S.T. Petcov, Phys. Rev. D 56 (1997) 5991; M. Maris, S.T. Petcov, Phys. Rev. D 56 (1997) 7444.
[67] E. Lisi, D. Montanino, Phys. Rev. D 56 (1997) 1792.
[68] E.Kh. Akhmedov, Nucl. Phys. B 538 (1999) 25.
[69] T. Ohlsson, H. Snellman, hep-ph/9912295.
[70] P.I. Krastev, S.T. Petcov, Phys. Lett. B 205 (1988) 84.
[71] J. Stoer, R. Bulirsch, Introduction to Numerical Analysis, Springer, New York, 1992.
[72] Particle Data Group, C. Caso et al., Eur. Phys. J. C 3 (1998) 1.
[73] CERN library, http://www.cern.ch/orasisftp.cern.ch.
[74] GAMS, http://gams.nist.gov.
[75] J.N. Bahcall, Neutrino Astrophysics, Cambridge Univ. Press, Cambridge, 1989.
[76] W. Kwong, S.P. Rosen, Phys. Rev. D 51 (1995) 6159.
[77] J.N. Bahcall, P.I. Krastev, E. Lisi, Phys. Rev. C 55 (1997) 494.
[78] Y. Fukuda et al., Phys. Rev. Lett. 82 (1999) 2430.
[79] P.C. de Holanda, C. Pĕna-Garay, M.C. Gonzalez-Garcia, J.W.F. Valle, Phys. Rev. D 60 (1999) 093010.
[80] A.M. Gago, H. Nunokawa, R. Zukanovich Funchal, hep-ph/0007270.
[81] J.N. Bahcall, M. Kamionkowski, A. Sirlin, Phys. Rev. D 51 (1995) 6146.